Doppler-Free Spectroscopy of the Hyperfine Structure in Rubidium

Samuel James Bader
MIT Department of Physics
(Dated: March 18, 2013)

Here we examine the hyperfine structure of the $5^2S_{1/2}$ and $5^2P_{3/2}$ states of ^{87}Rb and ^{85}Rb using Doppler-free spectroscopic techniques. We discuss the theory and experimental procedures of the Doppler-free method, then determine the hyperfine coupling constants of both the $5^2S_{1/2}$ and $5^2P_{3/2}$ sublevels in both isotopes from analysis of the resulting spectra, and examine possible sources of errors and uncertainties. Results are in accordance with previously accepted determinations of Rubidium hyperfine structure.

The major goal of this experiment is the determination of the hyperfine coupling constants A and B of ^{87}Rb and ^{85}Rb via room-temperature Doppler-free saturated absorption spectroscopy.

I. BACKGROUND

I.1. Rubidium HFS

The pertinent level structure of Rubidium is depicted in Fig. 1. We are interested in the D_2 transition (780nm) between the ground state, $5S_{1/2}$, and the second excited state $5P_{3/2}$. Hyperfine structure (HFS) due to coupling between the nuclear and electronic magnetic moments splits the $5S_{1/2}$ and $5P_{3/2}$ levels into sublevels distinguished by their total (nuclear plus electronic) angular momentum quantum number, F.

In ^{87}Rb, hyperfine structure splits the $5S_{1/2}$ state into two levels separated by 6.8GHz, and the $5P_{3/2}$ state into four levels spaced by an order of 100-200MHz. In ^{85}Rb, which is the more abundant isotope (72% vs 28%), the structure is qualitatively identical, except that the F values are one larger and the splittings are typically about half as large (note the ground state splitting of 3.0GHz).

Splittings for a given state of a given isotope can be well approximated using two coupling coefficients: the isotropic coupling, A, and the anisotropic coupling B, in the following expression:

$$\Delta f = A\frac{C}{2} + B\frac{3C(C+1) - 4I(I+1)J(J+1)}{8I(2I-1)J(2J-1)} \qquad (1)$$

where $C = F(F+1) - J(J+1) - I(I+1)$. The goal of this experiment is to measure these couplings.

However, these splittings cannot be resolved by conventional spectroscopy at room temperature, because of Doppler broadening. The Boltzmann velocity distribution for the Rubidium gas gives a typical velocity component along the laser propagation axis of $\approx$ 240m/s, which is about a millionth of the speed of light. So typical atoms may see the lasers Doppler-shifted by a part in a million, that is, by hundreds of megahertz. A beam red-detuned (or blue-detuned) within the Doppler linewidth will still resonate with atoms moving at typical velocities

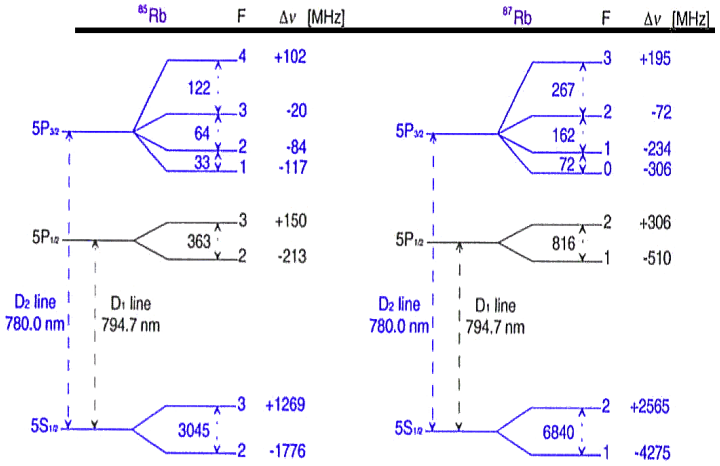

FIG. 1: Level struture of the two common Rubidium isotopes, ^{85}Rb and ^{87}Rb. Notice hyperfine splittings of 3.0GHz and 6.8GHz, respectively, in the ground states and tens or hundreds of MHz in the excited states. Modified from [1]

away from (or towards) the laser. More detailed calculations place the room temperature Doppler-broadened linewidth at 500MHz, which entirely obscures all of the hyperfine $5P_{3/2}$ splittings.

I.2. Doppler-free technique

This broadening can be eliminated by using two counterpropagating beams of differing intensities in order to select for only the zero-velocity group.

One beam, known as the "pump," is strong[1] enough to "saturate" the transition; of the atoms resonant with

[1] *Strong* compared to the saturation intensity,

$$I_{sat} = \frac{h\nu_0(1+\tau/T)}{2+\Gamma_i T}$$

where σ is the absorption cross section per atom, τ is the excited state lifetime, T is the duration for which a given atom is within the beam waist, and Γ_i is the sum of all spontaneous decay rates from the excited state out of the considered transition.

this beam, half will be excited, and half will be in the ground state. (Note that, because the rate coefficients of absorption and stimulated emission are identical, a laser cannot excite the population of a *two-level* system beyond saturation[2].)

The other beam, known as the "probe," and typically weaker by a factor of ten, is the beam whose transmission will be monitored. Let us consider the absorption profile of this beam. Following the depiction in Fig 2:

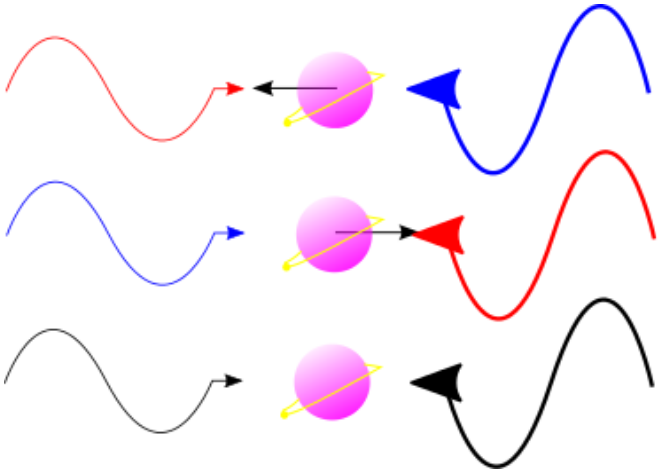

FIG. 2: Cartoon depiction of the Doppler-free scheme, probe on the left, pump on the right. Laser light is colored to represent the Doppler shift. A left moving atom *red-shifts* the probe (as shown), which means it will only absorb a *blue-detuned* probe.

(1) When the probe is blue-detuned, it will be absorbed by red-shifting (ie approaching) atoms. (2) When the probe is red-detuned, it will be absorbed by blue-shifting (ie fleeing) atoms. In both cases, the mentioned atoms will shift the pump in the opposite direction, so they will not simultaneously resonate with the pump. (3) When the probe is on transition, it resonates with atoms at rest, but so does the pump, and because the pump saturates the transition, half the atoms are already excited. Consequently, the probe stimulates just as much emission as absorption, and, overall, it transmits right through.

So we expect to see a broad ($\approx$ 500MHz) absorption peak, but with a small transmission dip (known as a Lamb dip) in the middle. The width of this peak is limited by the natural linewidth of the transition (or, in the case of this experiment, the laser linewidth $\approx$ 30MHz). Examples of Lamb dips will appear shortly.

[2] Excluding, of course, coherent effects (most famously Rabi flopping), which will damp out on the timescale of the spontaneous emission rate.

II. EXPERIMENTAL REALIZATION

The set-up used to apply this scheme is shown in Fig. 3. A laser controller allows the frequency of an external diode cavity laser to be swept over a range of several gigahertz. The output of this laser passes through a Faraday isolator which prevents undesirable feedback into the laser cavity, then onto the first beam splitter, wherein some of the light is diverted to a Fabry-Pérot cavity, used to monitor the frequency change in the laser during a sweep. The Fabry-Pérot was measured to have a length of 467 ± 3mm.[3]

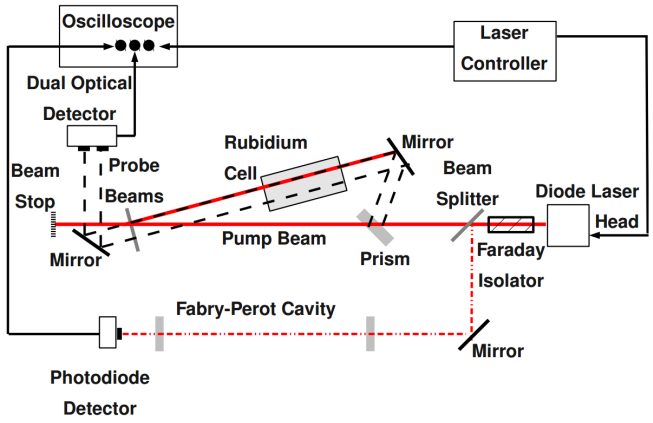

FIG. 3: The laser is split into two probes beams and one pump beam which counter-propagates along one of the probes. The difference of the two probe signals is passed to the oscilloscope. Image from [2].

The main beam continues to a prism: two reflections split off and become the probe beams, while the transmitted component becomes the pump. The probe beams are directed through the Rb vapor cell mutually parallel, and the pump is directed in the opposite direction through the cell along the same path as one of the probes. Thus one probe should be absorbed with a Doppler-broadened profile, and the other should have this profile but with the desired Lamb dips.

The transmission of both probes from the cell is directed unto a pair of balanced photodetectors, and their difference is sent to the oscilloscope. (The outputs of the individual probe beams are also sent to the scope for the purpose of debugging the setup). In total then, the scope will receive a Fabry-Pérot signal, for monitoring the frequency, the individual photodetector outputs and their

[3] The uncertainty in this trivial measurement comes from the difficulty of precisely locating the mirror interfaces which are shielded from side-long viewing by protective holders. In principle, of course, it is possible to determine the cavity length with much greater precision, however, this .06% uncertainty is already much smaller than other systematic sources, so reducing it would make no noticeable difference in our results.

balanced difference, a sweep signal from the laser controller, useful for monitoring the sweep, and an external trigger from the laser controller. Data is recorded and transferred to a computer for analysis.

III. DATA AND ANALYSIS

III.1. Frequency fitting

Since the $5S_{1/2}$ states have the larger splittings, transitions from each of the $5S_{1/2}$ states form their own groups, within which are peaks representing transitions to different excited $5P_{3/2}$ states. Output from a single frequency sweep is shown in Fig. 4, displaying all four peak groups simultaneously. Frequency increases from right to left, so, in that direction, the peaks represent transitions from ^{87}Rb $5S_{1/2}$, $F = 2$, then ^{85}Rb $5S_{1/2}$, $F = 3$, then ^{85}Rb $5S_{1/2}$, $F = 2$, and finally ^{87}Rb $5S_{1/2}$, $F = 1$. The first

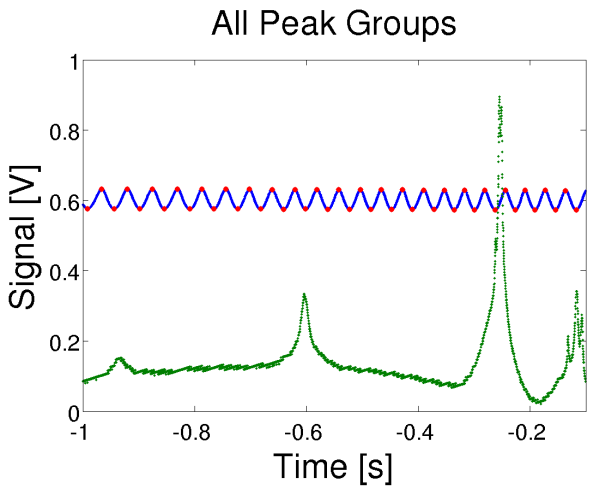

FIG. 4: Dataset showing all of the peak groups (green) and identified Fabry-Pérot peaks (red on blue). Note: irrelevant overall sloping removed for plot legibility.

step in analyzing a data set is to convert the time axis of the sweep into a frequency axis for the spectrum, using the Fabry-Pérot fringes. The algorithm devised for this purpose has several steps:

1. Fast Fourier Transform the Fabry-Pérot to estimate a typical peak-peak separation.

2. Supply that separation to a standard MATLAB peak-finding routine to locate all the maxima and minima.

3. Use those extrema as intial guesses for local sinusoidal fits to hone in on the precise location of each peak. (Results from this stage are displayed in Fig. 4 as the red dots; a plot like this is generated for each run so that the experimenter can confirm the procedure).

4. The frequencies at the peaks are known, and an (empirically motivated) quadratic fit of frequencies against time of peak generates a model for converting the time axis to a frequency axis. The RMS deviation is taken to estimate systematic frequency uncertainty. The results of this fit, for the same dataset, are shown in Fig 5. Note that is method of analysis has been modified from that given at a recent talk to address concerns raised in the Questions segment.

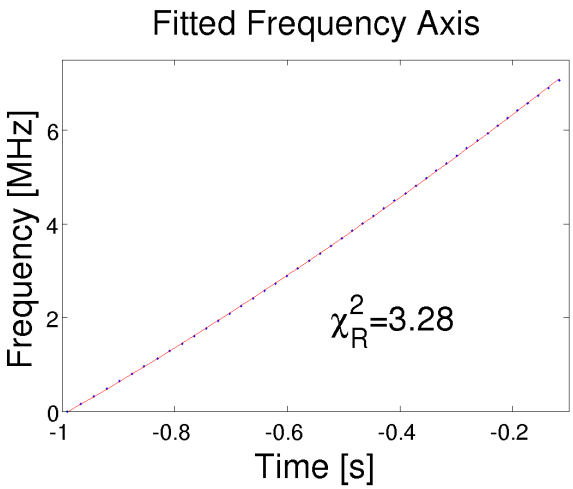

FIG. 5: Quadratic fit of sweeping frequency (obtained from Fabry-Pérot peaks) against time, used to convert the time axis of the oscilloscope to a frequency axis for analysis. This example comes from the same dataset as in Fig 4. (Error bars too small to appear.)

III.2. Peak Analysis within Peak Groups

Given the data on a frequency axis, we can now analyze the peak locations. A dataset corresponding to the rightmost peak of Fig. 4 is shown in Fig. 6. Regions of interest for each peak were selected manually, and then each peak was fit to a Lorentzian plus a linear function (the linear was added to reduce position bias due to sloping from the proximity of other peaks). Reasonable χ^2_R values justify this approach.

From these fits, one can then determine the interpeak distances, as given in Table I, and compare with calculated values. Note: all calculated values in this paper use Rubidium data from NIST [3]. The two sources of uncertainty at this point are systematic frequency uncertainty, as mentioned above, and fitting uncertainties.

As can be see in I, the systematic frequency uncertainty dominates within these small-window (ie individual peakgroup) datasets. However, this uncertainty can be reduced. Since it is due mainly to the non-linearity of the frequency sweep, we expect the errors to average

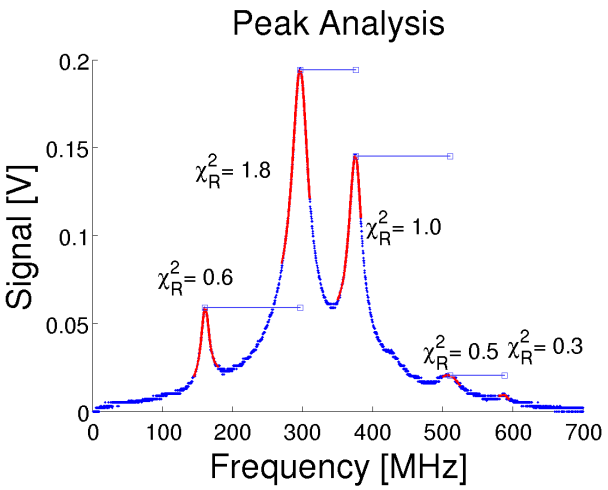

FIG. 6: Fitted peaks for the ^{87}Rb5S$_{1/2}$, F=2 group

$\Delta f_{\rm obs}$	$\sigma_{\rm stat}$	$\sigma_{\rm sys}$	$\Delta f_{\rm calc}$
135	.04	4	133
79	.07	4	78
135	.3	4	133
78	.5	4	78

TABLE I: Observed interpeak distances from Fig. 6, with statistical and systematic uncertainties, as compared to calculated values. All quantities in MHz.

out if the same peak separation is evaluated at multiple locations along the sweep. So if we take multiple spectra, with experimental conditions such that the peaks appear in different locations along the non-linear sweep, the systematic uncertainty should average down with a behaviour much like what one would expect from a statistical uncertainty ($\sigma \propto 1/\sqrt{n}$). Given that justification, we will estimate the systematic uncertainty of averaged interpeak distances by combining the frequency uncertainties in a statistical manner.[4]

If we take four different spectra such as the one in Fig 6 (totalling eight estimates for each separation at different locations along the sweep), and average the distances, and then do the same for the ^{85}Rb 5S$_{1/2}$, $F = 3$ group, we arrive at a final table of peak distances, which are in accordance with calculated values (see Table II).[5][6]

Isotope	Δf_{obs}	$\sigma_{\rm stat}$	$\sigma_{\rm sys}$	$\Delta f_{\rm calc}$
^{87}Rb	135.3	.02	1.4	133.3
^{87}Rb	79.5	.02	1.6	78.5
^{85}Rb	61.5	.2	.6	60.5
^{85}Rb	32.6	.1	.6	31.7

TABLE II: Averaged observed peak separations and their calculated values. All quantities in MHz. (Note: statistical errors for ^{87}Rb are much lower in proportion than for ^{85}Rb only because the ^{87}Rb peaks are more spaced and thus easier to fit.)

III.3. 5S$_{1/2}$ Coupling Determinations

Given these data, we are now in position to compute the couplings A and B for the the 5P$_{3/2}$ states. By evaluating (1) for each state, we can write the above interpeak distances as linear equations in terms of A and B, invert to solve for these couplings, and propagate the uncertainties through the linear system. The results, which agree with NIST values [3] within uncertainty, are compiled in Table III.

Isotope	State	A	$\sigma_{\rm stat}$	$\sigma_{\rm sys}$	B	$\sigma_{\rm stat}$	$\sigma_{\rm sys}$	$A_{\rm NIST}$	$B_{\rm NIST}$
^{87}Rb	5S$_{1/2}$	85.9	.02	1.4	12.8	.03	2.2	84.7	12.5
^{85}Rb	5S$_{1/2}$	25.4	.1	.5	26.1	.3	1.0	25.0	26.0

TABLE III: Observed and previously accepted values for the coupling constants of both isotopes of Rubidium. All quantities in MHz. (Note: the different scaling of the two types of errors between isotopes occurs for the same reason discussed under Table II).

III.4. Peak Analysis between Groups

The procedure to determine the coefficients for the 5S$_{1/2}$ states follows similarly, but relies on splittings between far distanced peaks rather than neighbors. Given that, a couple of minor differences in the details of the algorithm and its error propagation merit mention.

First, since we need to be able to see the individual peaks even when zoomed out to view the entire spectrum, the datasets for this analysis were collected with automatic scope averaging in order to improve the resolution. Unfortunately, this had the side effect of reducing/averaging down the intensity of the Fabry-Pérot (FP) signal, and the scope supplied this signal with less resolution than that with which it appeared. The discretization error in the FP fringes is noticable. However, since multiple spectra from this analysis were all taken *with*

[4] Also note that multiple peak separation values from each individual spectrum do correspond to the same underlying separation (see Table I), so each spectrum can give some degree of this averaging over the systematic uncertainty; ie each spectrum contributes multiple data points to the number of measurements of each separation.

[5] The two peaks mentioned are by far the best resolved, to such a degree that adding the other pair does not contribute significantly to this portion of the analysis. They will be used when discussing 5S$_{1/2}$ splittings.

[6] At this stage, we also linearly add in the .06% uncertainty due to Fabry-Pérot cavity measurement, which acts as an overall scaling factor in all the frequency differences.

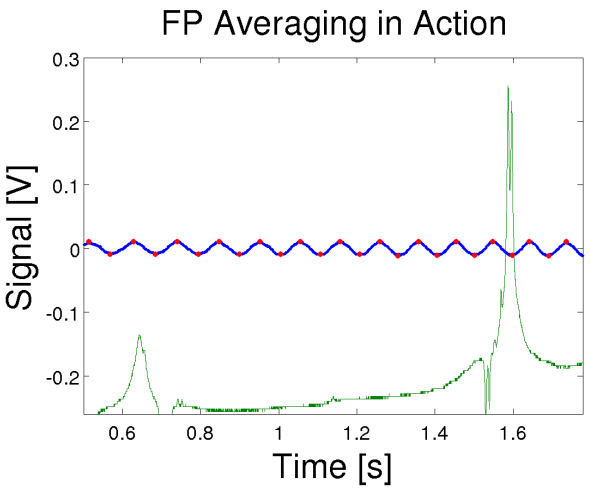

FIG. 7: Averaging together multiple Fabry-Pérot signals gives a clear enough signal to analyze.

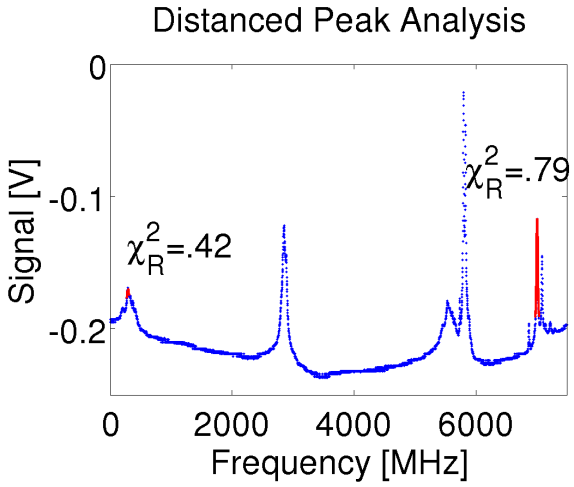

FIG. 8: Peaks from different groups are fit to Lorentzians with linear terms (to account for biasing for nearby peaks). This is exactly like the previous analysis.

the scope/sweep configuration in the same location, we have many FP signals for what should be the same spectrum (up to statistical errors), and by combining these Fabry-Pérot fringes together, we are able to reduce the discretization to the point where our basic peak-finding analysis is possible. This is demonstrated in Figure 7.

From there, a quadratic fit of frequency against time is performed just as before. Additional systematic uncertainty from our mentioned averaging procedure is taken into account by evaluating the the RMS deviation between FP peaks identifiable on individual data sets versus those located on the averaged dataset.

Then selected Lamb peaks are fit to Lorentzians with linear terms, just as before. An example is shown in Figure 8. Again, peak distances are averaged over multiple spectra. Note, however, that, in this case, the averaging does *not* reduce the systemic frequency uncertainty of the non-linear sweep, because all spectra being averaged were taken at the same postion on a sweep. So the frequency uncertainties here were not treated statistically: upon averaging the interpeak distances, the systematic uncertainties are simply averaged as well. (Of course, the actual statistical uncertainties from fitting are combined statistically). See Table IV.

Isotope	Δf_{obs}	σ_{stat}	σ_{sys}	Δf_{calc}
^{87}Rb	6707	4	74	6623
^{85}Rb	2969	9	5	2961

TABLE IV: Averaged observed peak separations and their calculated values. All quatities in MHz.

Isotope	State	A	σ_{stat}	σ_{sys}	A_{NIST}
^{87}Rb	$5P_{3/2}$	3461	2	61	3417
^{85}Rb	$5P_{3/2}$	1015	2.9	8.6	1012

TABLE V: The observed and the previously accepted values for the hyperfine couplies in the $5P_{3/2}$ states of both Rubidium isotopes.

Finally, we compute the couplings. The B coupling is irrelevant for the $5S_{1/2}$ states: the complicated coefficient of B in (1) is easily evaluated to be identically zero. So we take those averaged peak distances, and, combining their values with the appropriate $5P_{3/2}$ splittings determined earlier, we compute the A coupling for both isotopes, and propagate the errors through. With that, we arrive at the final table of A coefficients for the $5S_{1/2}$ states, Table V. Values agree with NIST data [3] within uncertainty.

IV. CONCLUSIONS

We have successfully measured the hyperfine coupling constants in the states of the D_2 transition in both common isotopes of Rubidium, and found values in agreement with previously accepted results to within one or two standard deviations. Future research may test this technique upon Zeeman splittings as well.

[1] Azmoun, Bob. Stonybrook University. http://laser.physics.sunysb.edu/~bazmoun/RbSpectroscopy
[2] MIT Junior Lab Guide: http://web.mit.edu/8.13/www/48.shtml
[3] Sansonetti. NIST. *Wavelengths, Transition Probabilities, and Energy Levels for the Spectra of Rubidium.* http://www.nist.gov/data/PDFfiles/jpcrd352006301.pdf